

# Solar Neutrino Oscillation – An Overview<sup>†</sup>

D.P. Roy

Tata Institute of Fundamental Research,  
Homi Bhabha Road, Mumbai 400 005, India

After a brief summary of the neutrino oscillation formalism and the solar neutrino sources and experiments I discuss the matter effect on solar neutrino oscillation. Then I discuss how the resulting alternative solutions are experimentally resolved in favour of the LMA solution, with particular emphasis on the SK, SNO and KL data.

<sup>†</sup>Plenary Talk at the Xth International Symposium on Particle, Strings and Cosmology (PASCOS), Boston, 16-22 August 2004.

The last four years have been widely described as the golden years of solar neutrino physics, thanks to three pioneering experiments – SuperKamiokande (SK), Solar Neutrino Observatory (SNO) and KamLAND (KL). They have provided for the first time a unique solution to the solar neutrino anomaly in terms of neutrino oscillation with unambiguous mass and mixing parameters. I shall give an overview of the subject with particular emphasis on the role of these experiments. After a brief summary of the neutrino oscillation formalism and the solar neutrino sources and experiments I shall discuss the matter effect on solar neutrino oscillation. We shall see how it leads to four alternative solutions to the solar neutrino anomaly and then their experimental resolution in favour of the so called Large Mixing Angle (LMA) solution over the last four years.

**Neutrino Mixing and Oscillation:** It was already noted by Pontecorvo back in the sixties that if the neutrinos have non-zero mass then there will in general be mixing between the flavour and the mass eigenstates, which will lead to neutrino oscillation [1]. We assume for simplicity two neutrino flavours, in which case mixing can be described by one angle  $\theta$ , i.e.

$$\begin{pmatrix} \nu_e \\ \nu_\mu \end{pmatrix} = \begin{pmatrix} \cos \theta & \sin \theta \\ -\sin \theta & \cos \theta \end{pmatrix} \begin{pmatrix} \nu_1 \\ \nu_2 \end{pmatrix}. \quad (1)$$

In fact it provides a very good approximation to the three neutrino mixing scenario for solar neutrino oscillation, with the second neutrino representing a mixture of the  $\nu_\mu$  and  $\nu_\tau$  flavours. Now each mass eigenstate propagates with its own phase

$$e^{-i(Et-p\ell)} \simeq e^{-\frac{im^2\ell}{2E}}, \quad (2)$$

where we have made the relativistic approximation,  $E = p + m^2/2p$ , since neutrino masses are much smaller than their kinetic energy. Thus a  $\nu_e$  produced at the origin will propagate as

$$\nu_e \rightarrow \nu_1 \cos \theta e^{-\frac{im_1^2}{2E}\ell} + \nu_2 \sin \theta e^{-\frac{im_2^2}{2E}\ell}. \quad (3)$$

Decomposing the  $\nu_{1,2}$  back into  $\nu_{e,\mu}$  after a distance  $\ell$  one sees that the  $\nu_\mu$  terms do not cancel, which implies neutrino oscillation. In fact the coefficient of the  $\nu_\mu$  term represents the probability of  $\nu_e \rightarrow \nu_\mu$  oscillation, i.e.

$$P_{\nu_e \rightarrow \nu_\mu}(\ell) = \left| \cos \theta \sin \theta \left( e^{-\frac{im_2^2}{2E}\ell} - e^{-\frac{im_1^2}{2E}\ell} \right) \right|^2$$

$$= \sin^2 2\theta \sin^2 \left( \frac{\Delta m^2}{4E} \ell \right), \quad (4)$$

where the first factor represents the amplitude and the second factor the phase of oscillation, with  $\Delta m^2 = m_1^2 - m_2^2$ . Converting to convenient units for  $\Delta m^2$  ( $eV^2$ ),  $\ell$  (m) and  $E$  (MeV) one gets

$$P_{\nu_e \rightarrow \nu_\mu}(\ell) = \sin^2 2\theta \sin^2(1.3\Delta m^2 \ell/E), \quad (5)$$

which corresponds to an oscillation wavelength

$$\lambda = \frac{\pi}{1.3} \cdot \frac{E}{\Delta m^2} \simeq 2.4E/\Delta m^2. \quad (6)$$

Thus for large mixing angle ( $\sin^2 2\theta \sim 1$ ) one expects the following pattern of oscillation probability from eqs. (5) and (6), where the factor of  $\frac{1}{2}$  in the last case comes from averaging over the phase factor.

$$\begin{array}{ccccccc} \ell & \ll \lambda & = \lambda/2 & \gg \lambda & & & \\ P_{\nu_e \rightarrow \nu_\mu} & 0 & \sin^2 2\theta \sim 1 & \frac{1}{2} \sin^2 2\theta \sim \frac{1}{2} & & & \end{array} \quad (7)$$

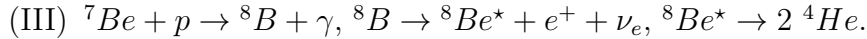
Note that the corresponding survival probability is given by the remainder, i.e.

$$P_{ee} \equiv P_{\nu_e \rightarrow \nu_e} = 1 - P_{\nu_e \rightarrow \nu_\mu}. \quad (8)$$

Now the typical energy of  $\nu_e$  coming from a nuclear reactor or the sun is  $\sim 1$  MeV. The typical distance between the source and the detector is a few hundred Km ( $\ell \sim 10^5$  m) for the long base line KamLAND reactor experiment, while  $\ell \sim 10^{11}$  m for solar neutrino experiments. Thus one sees from eqs. (6) and (7) that the KamLAND and the solar neutrino experiments can probe neutrino mass down to  $\Delta m^2 \sim 10^{-5}$   $eV^2$  and  $10^{-11}$   $eV^2$  respectively, which is far beyond the reach of any other method of mass measurement.

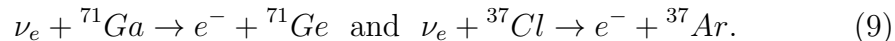
**Solar Neutrino Sources and Experiments:** The main sources of solar neutrinos are the  $pp$  chains of nuclear reaction, taking place at the solar core, which convert protons into  ${}^4He$  ( $\alpha$  particle). They are

- (I)  $pp \rightarrow {}^2H + e^+ + \nu_e$ ,  ${}^2H + p \rightarrow {}^3He + \gamma$ ,  ${}^3He + {}^3He \rightarrow {}^4He + 2p$ ; or
- (II)  ${}^3He + {}^4He \rightarrow {}^7Be + \gamma$ ,  ${}^7Be + e^- \rightarrow {}^7Li + \nu_e$ ,  ${}^7Li + p \rightarrow 2 {}^4He$ ; or



While most of this conversion takes place by the shortest path (I) a small fraction (15%) follows a detour via  ${}^7Be$  (II); and a tiny fraction (0.1%) of the latter follows a still longer detour via  ${}^8B$  (III). The resulting neutrinos are (I) the low energy  $pp$  neutrino, (II) the intermediate energy  $Be$  neutrino and (III) the relatively high energy  $B$  neutrino, with decreasing order of flux. The standard solar model (SSM) prediction for these fluxes is shown in Fig. 1 from BP 2000 [2]. It also shows the neutrino energy ranges covered by the different solar neutrino experiments.

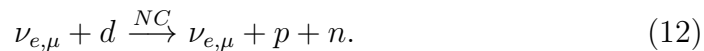
The Gallium [3] and the Chlorine [4] experiments are based on the charged current reactions



The produced  ${}^{71}Ge$  and  ${}^{37}Ar$  are periodically extracted by radiochemical method, from which the incident neutrino fluxes are estimated. The value of measured flux  $R$  relative to the SSM prediction gives the  $\nu_e$  survival probability  $P_{ee}$ . The SK is a real-time water Cerenkov experiment [5], based on the elastic scattering of neutrino on electron. The elastic scattering is dominated by the charged current reaction  $\nu_e + e^- \xrightarrow{CC} \nu_e + e^-$ , but it also has a limited sensitivity to the neutral current reaction  $\nu_{e,\mu} + e^- \xrightarrow{NC} \nu_{e,\mu} + e^-$ . Thus

$$R_{el} = P_{ee} + \frac{\sigma^{NC}}{\sigma^{NC+CC}}(1 - P_{ee}) \simeq P_{ee} + \frac{1}{6}(1 - P_{ee}). \quad (10)$$

This experiment can also measure the energy and direction of the incident neutrino from those of the outgoing electron. The SNO is a Cerenkov experiment with a heavy water target, which can detect both the charged and neutral current events [6-9]



In the 1st phase of the experiment the  $NC$  events were detected via neutron capture on deuteron,  $n + d \rightarrow t + \gamma$  [7]. In the 2nd phase salt was added to the heavy water target to enhance the  $NC$  detection efficiency via neutron capture on chlorine,  $n + {}^{35}Cl \rightarrow {}^{36}Cl + \gamma$  [8]. In the 3rd phase of this

experiment going on now  ${}^3\text{He}$  gas filled counters are inserted into the heavy water target to detect  $NC$  events via  $n + {}^3\text{He} \rightarrow t + p$  [9].

Table 1 shows the energy thresholds of the above four experiments along with the compositions of the corresponding solar neutrino spectra. It also shows the corresponding survival probability  $P_{ee}$  measured by the rates of the charged current reactions relative to the SSM prediction [2]. For the  $SK$  experiment the survival probability calculated from  $R_{e\ell}$  via eq. (10) is shown in parentheses. It shows that the survival probability is slightly above 1/2 for low energy  $\nu_e$ , falling to 1/3 at high energy. To understand its magnitude and the energy dependence we have to consider the effect of solar matter on neutrino oscillation.

**Table 1.** The  $\nu_e$  survival probability  $P_{ee}$  measured by the  $CC$  event rates of various solar neutrino experiments relative to the SSM prediction. For SK the  $P_{ee}$  obtained after NC correction is shown in bracket. The energy threshold and composition of neutrino beam are also shown for each experiment.

Experiment	Gallium	Chlorine	SK	SNO-I
R	$0.55 \pm 0.03$	$0.33 \pm 0.03$	$0.465 \pm 0.015$ ( $0.36 \pm 0.015$ )	$0.35 \pm 0.03$
$E_{th}$ (MeV)	0.2	0.8	5	5
Composition	$pp$ (55%), $Be$ (25%), $B$ (10%)	$B$ (75%), $Be$ (15%)	$B$ (100%)	$B$ (100%)

**Matter Enhancement (Resonant Conversion):** Propagation through solar matter gives an induced mass to  $\nu_e$ , which can have profound effect on neutrino oscillation. This is known as MSW effect after its authors [10]. It arises from the charged current interaction of  $\nu_e$  with solar electrons, while the neutral current interaction has no net effect since it is flavour independent. Adding this interaction energy density to the free particle wave equation gives

$$-i \frac{d}{dt} \begin{pmatrix} \nu_e \\ \nu_\mu \end{pmatrix} = \left( p + \frac{M^2 + 2EH_{int}}{2E} \right) \begin{pmatrix} \nu_e \\ \nu_\mu \end{pmatrix}, \quad (13)$$

where  $H_{int} = \sqrt{2}GN_e(0)$  for  $\nu_e(\nu_\mu)$ , with  $G$  and  $N_e$  denoting Fermi coupling and solar electron density. The quantity on the rhs numerator can be regarded as an effective mass or energy, i.e.

$$M'^2 = \begin{pmatrix} c & s \\ -s & c \end{pmatrix} \begin{pmatrix} m_1^2 & 0 \\ 0 & m_2^2 \end{pmatrix} \begin{pmatrix} c & -s \\ s & c \end{pmatrix} + \begin{pmatrix} 2\sqrt{2}EGN_e & 0 \\ 0 & 0 \end{pmatrix}$$

$$= \begin{pmatrix} c^2 m_1^2 + s^2 m_2^2 + 2\sqrt{2}EGN_e & -sc\Delta m^2 \\ -sc\Delta m^2 & c^2 m_2^2 + s^2 m_1^2 \end{pmatrix}, \quad (14)$$

where  $s, c$  denote  $\sin \theta, \cos \theta$ .

To get a simple picture let us assume for the moment that  $\sin \theta \ll 1$ , so that the nondiagonal elements are small. Then we can identify the two diagonal elements with the eigenvalues and the corresponding eigenstates  $\nu_{1,2}$  with the flavour eigenstates  $\nu_{e,\mu}$  respectively. Fig. 2 shows the two eigenvalues  $\lambda_{1,2}$  against the solar electron density. At the solar surface ( $N_e = 0$ ) the 1st eigenvalue ( $m_1^2$ ) is smaller than the 2nd ( $m_2^2$ ). But  $\lambda_1$  increases steadily with  $N_e$  and becomes much larger than  $\lambda_2$  at the solar core. The cross-over occurs at a critical density

$$N_e^c \equiv \frac{\Delta m^2}{2\sqrt{2}GE} \cos 2\theta, \quad (15)$$

corresponding to  $M'_{11} = M'_{22}$ . Note however that the two eigenvalues actually never cross. There is a minimum gap between them given by the nondiagonal element, i.e.

$$\Gamma = \Delta m^2 \sin^2 2\theta. \quad (16)$$

This means that a  $\nu_e$  produced at the solar core will come out as  $\nu_2$ , provided the transition probability between the two energy levels remains small.

It is easy to show that this remarkable result does not depend on the  $\sin \theta \ll 1$  assumption. Consider the effective mixing angle  $\theta_M$  in matter, which diagonalises the above matrix, i.e.

$$\tan 2\theta_M = \frac{2M'_{12}}{|M'_{22} - M'_{11}|} = \frac{\sin 2\theta}{|\cos 2\theta - 2\sqrt{2}GEN_e/\Delta m^2|}. \quad (17)$$

The electron density at the solar core is  $N_e^0 \gg N_e^c$ , so that the 2nd term in the denominator of eq. (17) is much larger than the 1st. This means  $\theta_M \ll 1$  at the solar core for any vacuum mixing angle  $\theta$ ; so that the  $\nu_e$  produced there is dominated by the  $\nu_1$  component. At the critical density the denominator of eq. (17) vanishes, which corresponds to maximal mixing between the two components, again for any value of  $\theta$ . This is why it is called matter enhanced (or resonant) conversion. It comes out from the sun as  $\nu_2$  with

$$P_{ee} = \sin^2 \theta, \quad (18)$$

provided the transition probability between the two levels remains small through out the propagation and in particular in the critical density region. This transition probability is given by the Landau-Zenner formula, i.e.

$$T = e^{-\frac{\pi}{2\gamma}}, \quad \gamma = \frac{\lambda(d\lambda_1/d\ell)_c}{\Gamma} \propto \lambda \frac{dN_e/d\ell}{N_e} \Big|_c, \quad (19)$$

where  $\lambda$  represents the oscillation wavelength in matter (which should not be confused with the eigenvalues  $\lambda_{1,2}$ ). If the solar electron density varies so slowly that the resulting variation in the 1st eigenvalue over an oscillation wavelength is small compared to the gap between the two, then  $\gamma \ll 1$  and the transition rate is exponentially suppressed. This is called the adiabatic condition. Thus the two conditions for the solar  $\nu_e$  to emerge as  $\nu_2$  can be written as

$$\frac{\Delta m^2 \cos 2\theta}{2\sqrt{2}GN_e^0} < E < \frac{\Delta m^2 \sin^2 2\theta}{2 \cos 2\theta (dN_e/d\ell N_e)_c}, \quad (20)$$

where the 1st inequality ensures  $N_e^0 > N_e^c$  and the 2nd one is the adiabatic condition.

Fig. 3 shows the triangular region in the  $\Delta m^2 - \sin^2 2\theta$  plot satisfying the above two conditions for a typical neutrino energy of  $E = 1$  MeV. The horizontal side follows from the 1st inequality, which gives a practically constant upper limit of  $\Delta m^2$  since  $\cos 2\theta \simeq 1$ . The 2nd inequality (adiabatic condition) gives a lower limit on  $\sin^2 2\theta$ . Moreover since this condition implies a lower limit on the product  $\Delta m^2 \sin^2 2\theta$ , it corresponds to the diagonal line on the log-log plot. The vertical side is simply given by the physical boundary, corresponding to maximal mixing. This is the so-called MSW triangle. The indicated survival probabilities outside the triangle follow from the vacuum oscillation formulae (7) and (8), while that inside is given by eq. (18). Thus  $P_{ee} < 1/2$  inside the MSW triangle and  $> 1/2$  outside it, except for the oscillation maximum at the bottom ( $\ell \simeq \lambda/2$ ) where  $P_{ee}$  goes down to  $\cos^2 2\theta$ . Finally the earth matter effect gives a small but positive  $\nu_e$  regeneration probability, which implies a day-night asymmetry – i.e. the sun shines a little brighter at night in the  $\nu_e$  beam. After day-night averaging one expects a  $\nu_e$  regeneration probability

$$\delta P_{reg} = \frac{\eta_E \sin^2 2\theta}{4(1 - 2\eta_E \cos 2\theta + \eta_E^2)}, \quad \eta_E = \frac{0.66}{\rho Y_e} \left( \frac{\Delta m^2/E}{10^{-13} \text{ eV}} \right), \quad (21)$$

where  $\rho$  is matter density in the earth in  $gm/cc$  and  $Y_e$  the average number of electrons per nucleon. For favourable values of  $\Delta m^2$  and  $\theta$   $\delta P_{reg}$  can go upto

0.15 as indicated in the Figure. It is important to note that the positions of the MSW triangle, the earth regeneration region and the vacuum oscillation maximum depend only on the ratio  $\Delta m^2/E$ , as one can see from the relevant formulae. Thus their positions on the right hand scale hold at all energies.

**Four Alternative Solutions:** Fig. 3 marks four regions in the mass and mixing parameter space, which can explain the magnitude and energy dependence of the survival probability  $P_{ee}$  shown in Table 1. They correspond to the so-called Large Mixing Angle (LMA), Small Mixing Angle (SMA), Low Mass (LOW) and Vacuum Oscillation (VAC) solutions. For the LMA and SMA solutions ( $\Delta m^2 \sim 10^{-5} \text{ eV}^2$ ) the low energy *Ga* experiment ( $E \ll 1 \text{ MeV}$ ) falls above the MSW triangle in  $\Delta m^2/E$ , while the SK and SNO experiments ( $E \gg 1 \text{ MeV}$ ) fall inside it. Therefore the solar matter effect can explain the observed decrease of the survival probability with increasing energy. For the LOW solution the low energy *Ga* experiment is pushed up to the region indicated by the dashed line, where it gets an additional contribution to the survival probability from the earth regeneration effect. Finally the VAC solution explains the energy dependence of the survival probability via the energy dependence of the oscillation phase in eq. (5). Fig. 4 shows the predicted survival probabilities of the four solutions as functions of neutrino energy. The LMA and LOW solutions predict mild and monotonic energy dependence, while the SMA and VAC solutions predict very strong and nonmonotonic energy dependence.

**Experimental Resolution in Favour of LMA:** The survival rates in Table 1 show a slight preference for a nonmonotonic energy dependence, since the intermediate energy Chlorine experiment shows a little lower rate than SK and SNO. Therefore the SMA and VAC were the favoured solutions in the early days. However the situation changed drastically with the measurement of the energy spectrum by SK [5], shown in Fig. 5. It shows very little energy dependence in clear disagreement with the predictions of the SMA and VAC solutions in Fig. 4. In particular the SMA solution in Fig. 4 can not reconcile a low survival rate of  $P_{ee} \simeq 1/3$  with an energy independent spectrum, in conflict with the SK data. The first charged current data from SNO [6] agreed with the low survival rate as well as the energy independent spectrum of the SK data. Thus the global analyses of the solar neutrino data at this stage ruled out the SMA and VAC solutions in favour of LMA and LOW [11].



Then came the first neutral current data from SNO [7]. Being flavour independent the neutral current reaction is unaffected by neutrino oscillation. Hence it can be used to measure the Boron neutrino flux, for which the SSM has a large uncertainty (see Fig. 1). The SNO neutral current measurement of this flux was in agreement with the SSM prediction and significantly more precise than the latter. Fig. 6 shows the results of global fit with and without the SNO (NC) data [12]. The left and the middle panels show two different methods of using the NC data and give very similar results. They strongly favour the LMA solution while barely allowing LOW at  $3\sigma$  level. The reason is that the earth regeneration contribution is too small to account for the large survival rate of the *Ga* compared to those of the SK and SNO (CC) experiments. Without the SNO (NC) data it was possible to effectively push up the survival rate of the latter experiments from 0.35 to 0.45 by exploiting the large uncertainty in the Boron neutrino flux, and hence accommodate the LOW solution as shown in the right panel (see also Fig. 4). However this was no longer possible after the SNO (NC) data [12,13] due to the improved precision of the Boron neutrino flux.

**Confirmation and Sharpening of the LMA Solution:** Independent confirmation of the LMA solution came from the reactor antineutrino data of the KamLAND experiment [14], assuming CPT invariance. It is a 1 kiloton liquid scintillator experiment detecting  $\bar{\nu}_e$  from the Japanese nuclear reactors via

$$\bar{\nu}_e + p \rightarrow e^+ + n. \quad (22)$$

It also measures the incident  $\bar{\nu}_e$  energy  $E$  via the visible scintillation energy produced by the positron and its annihilation with a target electron, i.e.

$$E_{vis} = E + m_e + m_p - m_n = E - 0.8 \text{ MeV}. \quad (23)$$

The mean base line distance of the detector from the reactors is  $\langle \ell \rangle \sim 180$  km, which means it is sensitive to the  $\Delta m^2 \gtrsim 10^{-5} \text{ eV}^2$  region as mentioned earlier. Thus the experiment was designed to probe the LMA region. It was shown in [15] that if the survival rate seen at KL is  $< 0.9$ , then it would rule out the LOW solution at  $3\sigma$  level. The first KL result from 162ty data showed a survival rate  $R = 0.611 \pm .085 \pm .041$  [14]. This was in perfect agreement with the LMA prediction and ruled out LOW at  $5\sigma$  level. Moreover the observed spectral distortion of the KL data, taken together with global solar neutrino data, confined the LMA solution to two subregions around  $\Delta m^2 = 7$  and

$14 \times 10^{-5} \text{ eV}^2$ , as shown in Fig. 7 [16]. They correspond to the 1st and 2nd oscillation minima ( $\langle \ell \rangle = \lambda$  and  $2\lambda$ ) for  $E_{vis} \simeq 4.5 \text{ MeV}$ , where the observed spectrum touches the no-oscillation prediction (see Fig. 9). The best fit point lies in the lower region called LMA-I, while LMA-II is allowed only at 99% CL [16,17].

This was followed by the data from the second (salt) phase of SNO [8], with better  $NC$  detection efficiency. Combining the data from the two phases in a global analysis helped to constrain the mass and mixing parameters further [18,19]. Fig. 8 shows the results of global fits with phase-1, phase-2 and the combined SNO data [18]. The combined fit is seen to allow the LMA-II region only at  $3\sigma$  and disallow maximal mixing at  $5\sigma$ . The most important issue at this point was a definitive resolution of the LMA-I and II ambiguity. It was shown through a simulation study in [18] that if the KL spectrum from 1 kty data continues to favour the LMA-I region, then combining this with the global solar neutrino data will rule out LMA-II at  $> 3\sigma$  level.

Recently the KL experiment has published their 766 ty data, whose best fit point is indeed in the LMA-I region [20]. Combining this with the global solar neutrino data rules out LMA-II at  $> 3\sigma$  while sharpening the LMA-I region further [21,22]. Fig. 9 compares the KL spectrum with the no-oscillation and oscillation best fit predictions. Fig. 10 shows the result of combined fit to the KL and global solar neutrino data [21]. The 90% CL contour of the global solar fit is shown for comparison. In comparing the two 90% CL contours we see that the mass parameter is mainly determined by the KL data, while the mixing angle is determined mainly by the solar neutrino data. The best fit values along with  $1\sigma$  errors are

$$\Delta m^2 = (8.0 \pm .6) \times 10^{-5} \text{ eV}^2, \quad \sin^2 \theta = 0.28 \pm .03. \quad (24)$$

The best fit value of  $\Delta m^2$  corresponds to the 1st oscillation minimum ( $\lambda = \langle \ell \rangle = 180 \text{ km}$ ) occurring at  $E_{vis} \simeq 5 \text{ MeV}$ , in agreement with Fig. 9. It is evident from eq. (24) and Fig. 10 that the solar neutrino oscillation has finally entered the arena of precision physics.

**Concluding Remarks:** Oscillation analysis of global solar neutrino plus KL data has been extended to three neutrino flavours [21]. The resulting mass and mixing parameters agree very well with those of the two-flavour analysis discussed above. Moreover dropping one of the solar neutrino experiments from the global analysis is also found to make little difference to the result.

Thus the results are stable and robust. As regards future prospects, the precision of  $\Delta m^2$  will improve further with accumulation of more KL data. One expects some improvement in the precision of the mixing angle from the 3rd phase of SNO, but not from KL. The main reason for this is the occurrence of an oscillation minimum in the middle of the  $\bar{\nu}_e$  spectrum ( $E_{vis} \simeq 5$  MeV). This means that the coefficient of  $\sin^2 2\theta$  in the oscillation probability (eq. 5) is very small over this energy range. An interesting suggestion made in [23] is to reduce the base line length by half ( $\sim \lambda/2$ ), which would mean an oscillation maximum in the middle of the  $\bar{\nu}_e$  spectrum instead. A KL type experiment at a reduced base line length of  $\sim 70$  km has been estimated to improve the precision of  $\sin^2 \theta$  significantly.

It is my pleasure to thank the organisers of PASCOS'04 for their invitation and kind hospitality. Let me also take this opportunity to thank my teammates Abhijit Bandyopadhyay, Sandhya Choubey and Srubabati Goswami.

## References

1. B. Pontecorvo, Zh. Eksp. Teor. Fiz. 53 (1967) 1717.
2. J.N. Bahcall, M.H. Pinsonneault and S. Basu, *Astrophys J.* 555 (2001) 990; <http://www.sns.ias.edu/~jnb>.
3. SAGE: J.N. Abdurashitov et al., *JETP* 95 (2002) 181;  
GALLEX: W. Hampel et al., *Phys. Lett.* B447 (1999) 127;  
GNO: C. Cattadori, Talk at Neutrino 2004, Paris (2004).
4. B.T. Cleveland et al., *Astro Phys. J.* 496 (1998) 505.
5. SK Collaboration: S. Fukuda et al., *Phys. Lett.* B539 (2002) 179.
6. SNO: Q.R. Ahmad et al., *Phys. Rev. Lett.* 87 (2001) 071301.
7. SNO: Q.R. Ahmad et al., *Phys. Rev. Lett.* 89 (2002) 011301 & 011302.
8. SNO: S.N. Ahmed et. al., arXiv: nucl-ex/0309004.
9. SNO: H. Robertson, Talk at TAUP 2003, Seattle (2003).
10. L. Wolfenstein, *Phys. Rev.* D17 (1978) 2369; S.P. Mikheyev and A.Y. Smirnov, *Sov. J. Nucl. Phys.* 42 (1985) 913 [*Yad. Fiz.* 42 (1985) 1441].
11. A. Bandyopadhyay, S. Choubey, S. Goswami and K. Kar, *Phys. Lett.* B519 (2001) 83; G.L. Fogli, E. Lisi, D. Montanino and A. Palazzo, *Phys. Rev.* D64 (2001) 093007; J.N. Bahcall, M.C. Gonzalez-Garcia and C. Pena-Garay, *JHEP* 0108 (2001) 014; P.I. Krastev and A.Y. Smirnov, *Phys. Rev.* D65 (2002) 073002.
12. A. Bandyopadhyay, S. Choubey, S. Goswami and D.P. Roy, *Phys. Lett.* B540 (2002) 14.
13. V. Barger, D. Marfatia, K. Whisnant and B.P. Wood, *Phys. Lett.* B537 (2002) 179; J.N. Bahcall, M.C. Gonzalez-Garcia and C. Pena-Garay, *JHEP* 0207 (2002) 054; P.C. de Holanda and A.Y. Smirnov, *Phys. Rev.* D66 (2002) 113005; A. Strumia, C. Cattadori, N. Ferrari and F. Vissani, *Phys. Lett.* B541 (2002) 327.

14. KamLAND: K. Eguchi et al., Phys. Rev. Lett. 90 (2003) 021802.
15. A. Bandyopadhyay, S. Choubey, R. Gandhi, S. Goswami and D.P. Roy, J. Phys. G29 (2003) 2465.
16. A. Bandyopadhyay, S. Choubey, R. Gandhi, S. Goswami and D.P. Roy, Phys. Lett. B559 (2003) 121.
17. G.L. Fogli et al., Phys. Rev. D67 (2003) 073002; M. Maltoni, T. Schwetz and J.W. Valle, Phys. Rev. D67 (2003) 093003. J.N. Bahcall, M.C. Gonzalez-Garcia and C. Pena-Garay, JHEP 0302 (2003) 009; P.C. de Holanda and A.Y. Smirnov, JCAP 0302 (2003) 001.
18. A. Bandyopadhyay, S. Choubey, S. Goswami, S.T. Petcov and D.P. Roy, Phys. Lett. B583 (2004) 134.
19. G.L. Fogli, E. Lisi, A. Marrone and A. Palazzo, Phys. Lett. B583 (2004) 149; P.C. de Hollanda and A.Y. Smirnov, Astropart. Phys. 21 (2004) 287.
20. KamLAND: T. Araki et al., arXiv: hep-ex/0406035.
21. A. Bandyopadhyay, S. Choubey, S. Goswami, S.T. Petcov and D.P. Roy, arXiv:hep-ph/0406328.
22. J.N. Bahcall, M.C. Gonzalez-Garcia and C. Pena-Garay, JHEP 0406 (2004) 016; O. Miranda, M. Tartola and J.W. Valle, arXiv; hep-ph/0406280.
23. A. Bandyopadhyay, S. Choubey and S. Goswami, Phys. Rev. D67 (2003) 113011.

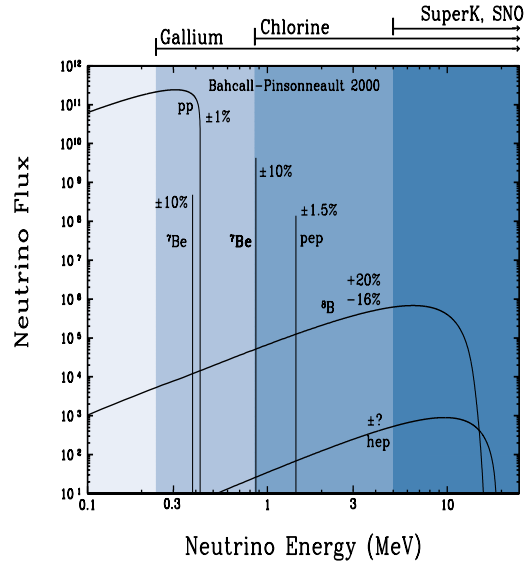


Figure 1: The SSM prediction for the solar neutrino fluxes is shown along with the energy ranges of the solar neutrino experiments [2].

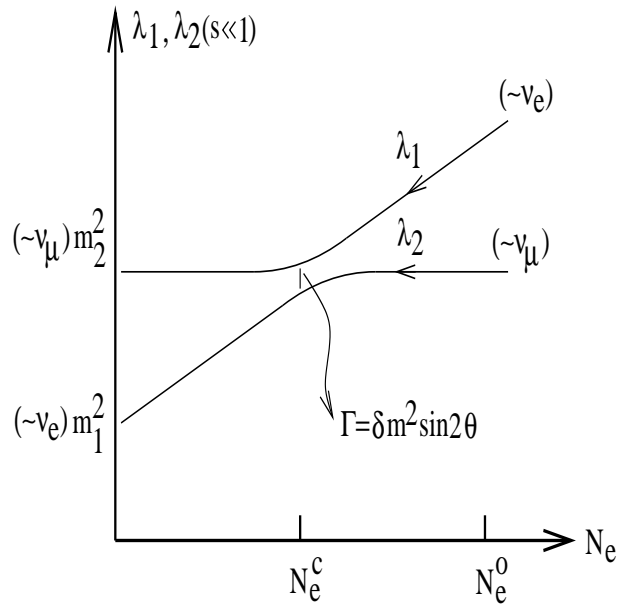


Figure 2: Schematic diagram of the effective mass (energy) eigenvalues of  $\nu_{e,\mu}$  as functions of the solar electron density.

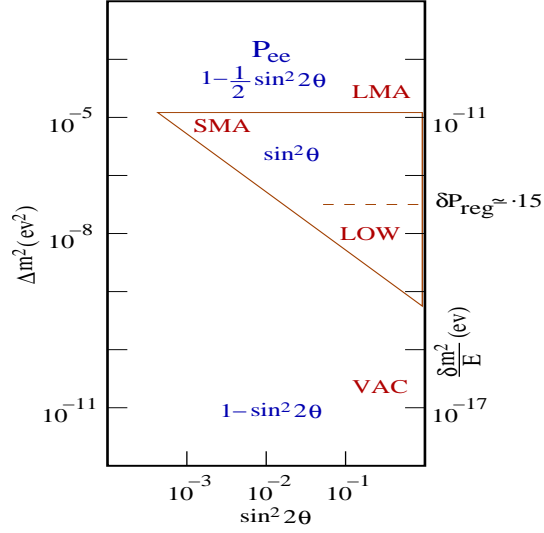


Figure 3: The positions of the MSW triangle, the earth regeneration effect and the vacuum oscillation maximum at  $E = 1$  MeV are shown along with those of the SMA, LMA, LOW and VAC solutions. While the former positions scale with  $E$  the latter ones are independent of it.

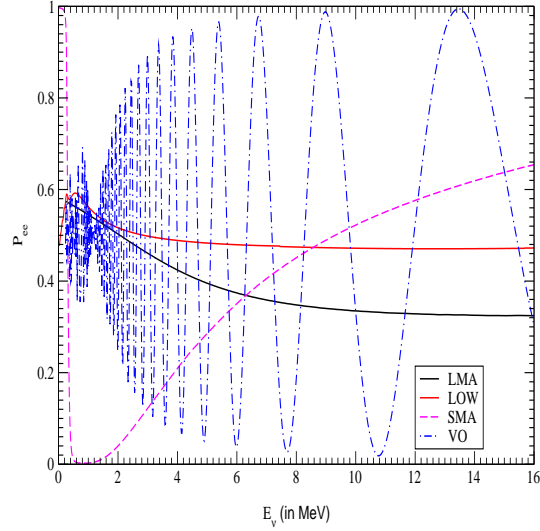


Figure 4: The predicted  $\nu_e$  survival probabilities (rates) for the SMA, LMA, LOW and VAC solutions.

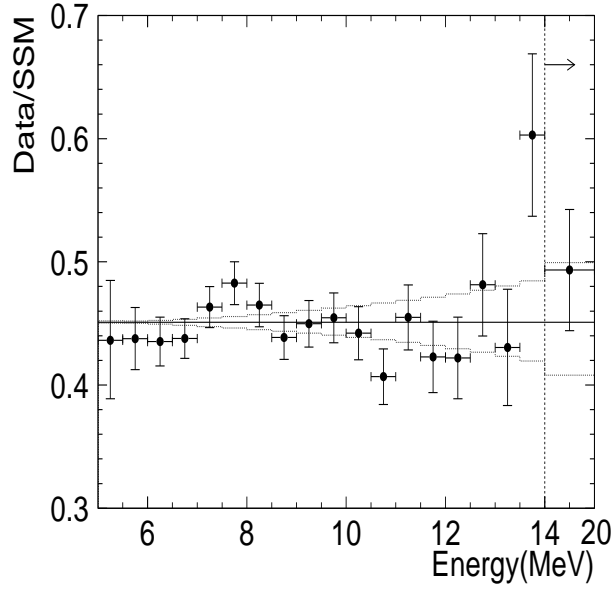


Figure 5: The energy (in)dependence of the SK spectrum [5].

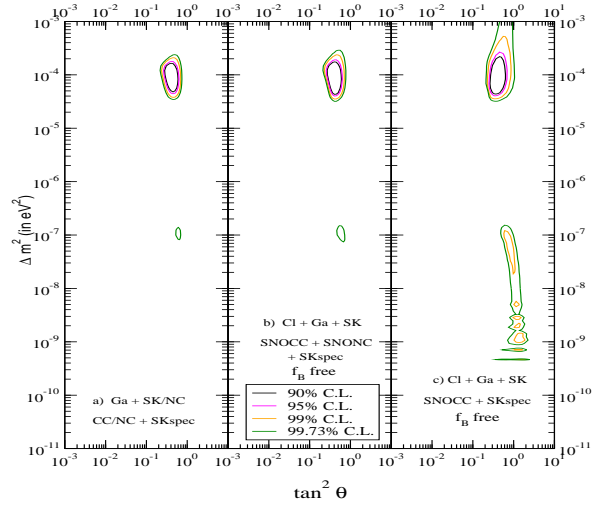


Figure 6: Results of global solar neutrino data fits with (left and middle) and without (right panel) the first SNO neutral current data [12].



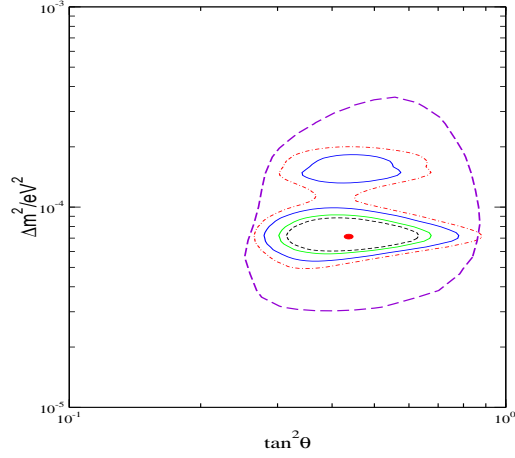


Figure 7: The 90,95,99 and 99.73% CL contours of global fit to solar neutrino plus the 162 ty KL data. The 99.73% CL ( $3\sigma$ ) contour of the solar fit is shown for comparison [16].

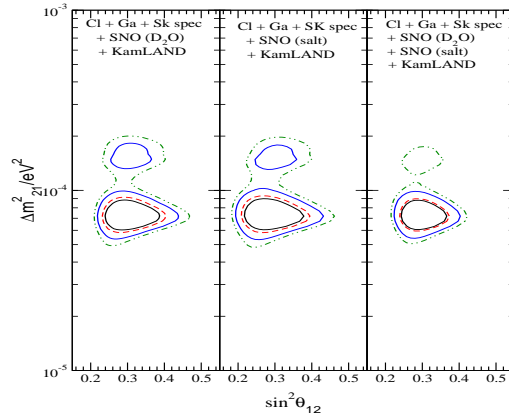


Figure 8: The 90,95,99 and 99.73% CL contours from global fits to solar neutrino plus 162 ty KL data with phase-I, phase-II and combined SNO data [18].

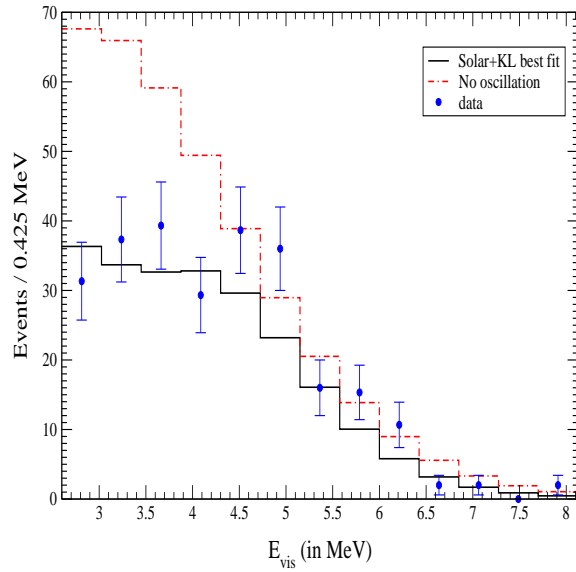


Figure 9: The 766 ty KL spectrum compared with the no-oscillation and oscillation best fit predictions [21].

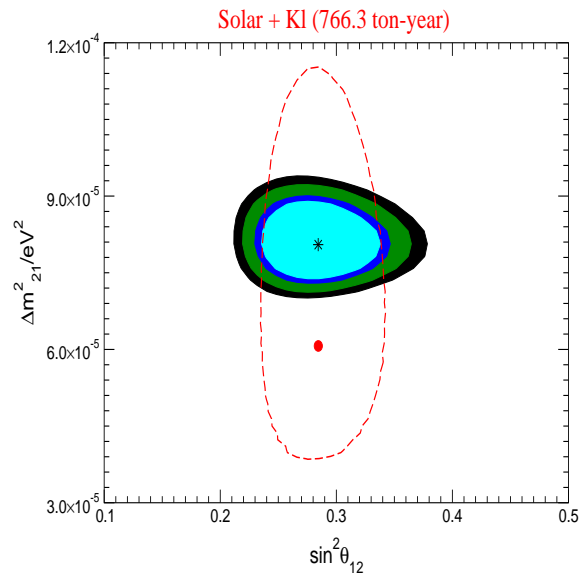


Figure 10: The 90,95,99 and 99.73% contours from global fit to solar neutrino plus 766 ty KL data. The 90% CL contour of the solar fit is shown for comparison [21].